Bose-Einstein condensation in diamond hierarchical lattices

M. L. Lyra,[1] F. A. B. F. de Moura,[1] I. N. de Oliveira,[1] and M. Serva[2,*]

[1]*Instituto de Física, Universidade Federal de Alagoas, 57072-900 Maceió-AL, Brazil*
[2]*Departamento de Biofísica e Farmacologia, Universidade Federal do Rio Grande do Norte, 59072-970 Natal-RN, Brazil*

The Bose-Einstein condensation of noninteracting particles restricted to move on the sites of hierarchical diamond lattices is investigated. Using a tight-binding single-particle Hamiltonian with properly rescaled hopping amplitudes, we are able to employ an orthogonal basis transformation to exactly map it on a set of decoupled linear chains with sizes and degeneracies written in terms of the network branching parameter q and generation number n. The integrated density of states is shown to have a fractal structure of gaps and degeneracies with a power-law decay at the band bottom. The spectral dimension d_s coincides with the network topological dimension $d_f = \ln(2q)/\ln(2)$. We perform a finite-size scaling analysis of the fraction of condensed particles and specific heat to characterize the critical behavior of the BEC transition that occurs for $q > 2$ ($d_s > 2$). The critical exponents are shown to follow those for lattices with a pure power-law spectral density, with non-mean-field values for $q < 8$ ($d_s < 4$). The transition temperature is shown to grow monotonically with the branching parameter, obeying the relation $1/T_c = a + b/(q - 2)$.

I. INTRODUCTION

The thermodynamic behavior of model systems embedded in complex networks has attracted the interest of the scientific community over the past three decades [1–25], due to the possibility of using powerful analytical techniques to provide exact results for the thermodynamic properties of interacting particles systems in lattices with discrete scale invariance. A prominent example is the use of exact Migdal-Kadanoff renormalization-group approach in hierarchical diamond lattices [1–4], where it was demonstrated that many models of interacting spins with nearest neighbor couplings are exactly solvable [2]. In particular, reported in detail was the topological properties of the diamond hierarchical lattice and its thermodynamic signatures, with the free energy exhibiting a well-defined thermodynamic limit for a large class of discrete spin models [2]. Moreover, it was also shown that these lattice models provide numerous examples of phase coexistence and critical points at finite temperatures, including cases of continuously varying critical exponents [3].

A historical question concerns whether calculations on hierarchical lattices provide genuine insights into phase transitions for the corresponding models on Bravais lattices. Previous reports pointed out the similarities and differences between the thermodynamic properties of hierarchical lattices and their corresponding Bravais-lattice models [4]. Further, it was demonstrated that the phase diagram for the polymerization problem on the diamond hierarchical lattice is the same as that expected for regular lattices [5]. In this context, the properties of the phase transitions and their universality classes have been investigated in a family of diamond-type hierarchical lattices on which the Ising model is exactly solved [7]. Considering both regular and fractal lattices, general criteria for the classification of the universality classes were proposed in which certain geometric factors were introduced to distinguish

the critical behavior in regular and fractal lattices [7]. By using a refined transfer-matrix procedure to investigate a disordered short-range Ising model on the diamond hierarchical lattice, the thermodynamic functions and the phase diagram were obtained on the basis of the behavior of the correlation length [14]. The critical behavior was also investigated in the random q-state Potts model in the large-q limit on a diamond hierarchical lattice, where it was observed that the ferromagnetic-paramagnetic phase transition is controlled by four different fixed points [10]. Moreover, it was reported that a spin-glass condensation transition takes place in a non-mean-field model, consisting in a hierarchical lattice where the interaction strength between variables is a decreasing function of their mutual hierarchical distance [13].

Recently, several works have been devoted to the investigation of the thermodynamic behavior of ideal quantum gases on complex networks [16–20,22,23,25,26]. In particular, it was observed that the network topology plays a predominant role in the thermodynamic properties of ideal quantum gases, especially in the Bose-Einstein condensation phenomenon (BEC). The ideal Bose gas on star and comb graphs has been shown to display a condensation transition due to the presence of hidden states in the bottom of the energy spectrum [18–20,22,23]. By using a tight-binding approach for noninteracting bosons, the topology-induced Bose-Einstein condensation has also been demonstrated to take place in the deterministic scale-free Apollonian network [17], with the transition temperature and the gap between the ground and first excited states exhibiting the same diverging finite-size scaling law. Such a diverging scaling behavior is associated with the enhancement in the number of connections as new generations are included at the Apollonian network, thus leading to a diverging energy bandwidth and an ill-defined thermodynamic limit. However, a proper rescaling of the tight-binding parameters regularizes the energy spectrum [25,26], providing the characterization of the critical behavior of the condensed fraction, correlation size, and specific heat. More specifically, the critical exponents and the power-law behavior of the density of states near the band bottom indicated that the BEC condensation in the Apollonian

---
*On leave from DISIM, Università dell'Aquila, 67010 L'Aquila, Italy.

network belongs to the universality class of the ideal BEC in lattices with spectral dimension $d_s \approx 3.74$. Therefore, hierarchical scale-free networks appear as prototype lattice geometries on which analytical and numerical techniques can be employed to explore the critical behavior of the BEC transition.

In this work, we provide the exact solution for the thermodynamic behavior of the ideal Bose gas in a family of hierarchical diamond lattices with varying fractal dimensions. After a proper change of the orthonormal basis, we show that the single-particle tight-binding Hamiltonian on diamondlike lattices can be written as a set of noninteracting Hamiltonians on linear chains with distinct sizes and degeneracies. In particular, we show that the resulting energy spectrum exhibits a fractal distribution of minibands and gaps, with the overall spectral dimension coinciding with the underlying fractal dimension of the lattice. From the exact single-particle energy spectrum, we determine the thermodynamic properties of the ideal Bose gas on such family of hierarchical networks whose critical behavior can be tuned from non-mean-field to mean-field-like by changing the geometric aspect of the elementary lattice cell.

II. DIAMOND HIERARCHICAL LATTICES

In this work, we will consider a gas of noninteracting bosons occupying the sites of a diamond hierarchical lattice. Such lattice is constructed recursively starting from a single link corresponding to the generation $n = 0$. The generation $n = 1$ consists of q branches in parallel, each one containing two bonds in series (see Fig. 1). The next generation $n = 2$ is obtained by applying the same transformation to each bond of the generation $n = 1$. At generation n, the length L_n measured by the number of bonds between the two extreme sites is $L_n = 2^n$, and the total number of bonds is $U_n = (L_n)^{d_f}$ where $d_f = \ln(2q)/\ln(2)$ represents the effective dimensionality.

A. Some numbers

At generation $n = 0$ the diamond has two nodes and one bond. Here we will consider diamond fractals with q legs. At each new generation, a bond gives rise to q new nodes and it is replaced by $2q$ new bonds. Therefore, if N_n is the number of nodes at generation n and U_n is the number of bonds,
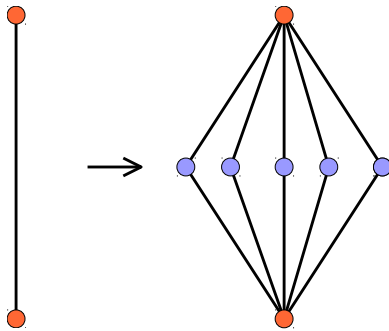

FIG. 1. (Color online) Schematic representation of the construction of the first generation of the diamond hierarchical lattice with $q = 5$ branches from the generation 0 lattice.

one has

$$N_{n+1} = N_n + q\,U_n, \quad U_{n+1} = 2q\,U_n \tag{1}$$

with initial conditions $N_0 = 2$ and $U_0 = 1$. At generation n, the solution is

$$N_n = \frac{q\,(2\,q)^n + 3\,q - 2}{2\,q - 1}, \quad U_n = (2\,q)^n \tag{2}$$

for large q the number of nodes is proportional to the number of bonds ($N_n \simeq \frac{q}{2q-1}\,U_n$).

The connectivity of the two initial nodes of generation $n = 0$ equals 1, furthermore, the connectivity of each existing node is updated by a factor q at any new generation and the connectivity of each new created node equals 2. Therefore, connectivities can take only the values $2\,q^m$ with $0 \leqslant m \leqslant n - 1$ and q^n (for the two initial nodes). More precisely, the number $N_n(k)$ of nodes with connectivity k is 2 if $k = q^n$, $N_n(k) = q\,(2\,q)^{n-m-1}$ if $k = 2\,q^m$ and 0 otherwise. Obviously,

$$\sum_{k=0}^{\infty} N_n(k) = 2 + \sum_{m=0}^{n-1} q\,(2\,q)^{n-m-1} = N_n. \tag{3}$$

The average connectivity is $\bar{k}$ is given by

$$\bar{k} = \frac{1}{N_n} \sum_{k=0}^{\infty} N_n(k)\,k = \frac{1}{N_n}[2\,q^n + n\,q\,(2\,q)^{n-1}] \tag{4}$$

which, given $N_n \simeq \frac{q}{2q-1}\,(2q)^n$, implies $\bar{k} \simeq c_q\,n$ for large n. Notice that $c_q = (2q - 1)/2q$ slowly increases with q and it is always smaller than unity.

B. Tight-binding Hamiltonian and its energy spectrum

The tight-binding model is defined assuming that the single-particle Hamiltonian on the diamond network of generation n is

$$H_n = \sum_{i,j} \frac{2t}{\sqrt{k_i\,k_j}} (|i\rangle\langle j| + |j\rangle\langle i|), \tag{5}$$

where $2t$ is the hopping energy and k_i, k_j indicate the connectivity of nodes i and j respectively. Such rescaling of the hopping amplitudes is essential to regularize the energy spectrum in the thermodynamic limit [25,26]. The sum goes on all bond-connected pairs of nodes (therefore, the sum goes on all U_n possible bonds). The number of eigenvalues of the Hamiltonian must equal the number of states $|i\rangle$ which, in turn, equals the number N_n of nodes i.

An analytical approach based on a change of basis can decouple the Hamiltonian into several uncoupled, noninteracting parts. Such scheme has been previously used to reveal the possibility of an insulator-metal crossover in a class of disordered systems in quasi-one dimension as well as in two dimensions [27–29]. We show (see the Appendix) that after a proper change of the orthonormal basis, the Hamiltonian can be rewritten as

$$H_n = \sum_{m=1}^{n-1} \sum_{r=1}^{g(m)} \Gamma_{r,m} + \sum_{r=1}^{q-2} \Gamma_{r,n} + \Gamma_{n+1}, \tag{6}$$

where $g(m) = (q - 1)(2q)^{n-m}$ and the system is decomposed in noninteracting parts, each of them associated to one of

the different $\Gamma_{r,m}$ or to Γ_{n+1}. The auxiliary Hamiltonians $\Gamma_{r,m}$ correspond to open chains of length $2^m - 1$ and hopping energies t, i.e.,

$$\Gamma_{r,m} = t \sum_{l=1}^{2^m-2} (|m,r,l\rangle\langle m,r,l+1| + |m,r,l+1\rangle\langle m,r,l|), \quad (7)$$

where different pairs of r,m corresponds to different chains. Notice that the $\Gamma_{r,1}$ are vanishing Hamiltonians corresponding to isolated points. Furthermore, the auxiliary Hamiltonian Γ_{n+1} corresponds to a closed chain of length 2^{n+1} and hopping energies t, i.e.,

$$\Gamma_{n+1} = t \sum_{l=1}^{2^{n+1}} |n+1,1,l\rangle\langle n+1,1,l+1|$$

$$+ \sum_{l=1}^{2^{n+1}} |n+1,1,l+1\rangle\langle n+1,1,l| \quad (8)$$

with the periodic condition $|n+1,1,l\rangle = |n+1,1,l+2^{n+1}\rangle$. The noninteractivity of the various parts of the Hamiltonian is assured by the orthonormality conditions $\langle a,b,c|a',b',c'\rangle = \delta_{a,a'}\delta_{b,b'}\delta_{c,c'}$ where δ indicates the Kronecker δ and a,b,c,a',b',c' can take all possible values corresponding to (7) and (8).

Since the $\Gamma_{r,m}$ have $2^m - 1$ eigenvalues and Γ_{n+1} has 2^{n+1} eigenvalue, the total number of eigenvalues is $\sum_{m=1}^{n-1} g(m)(2^m - 1) + (q - 2)(2^n - 1) + 2^{n+1} = N_n$ as it must be.

The full spectrum of eigenenergies can be directly obtained by recalling that, for an open chain of length L, they are given by

$$E_n = 2t \cos \frac{2\pi n}{L+1}, \quad n = 1, 2, \dots, L, \quad (9)$$

while the eigenenergies for a closed chain are

$$E_n = 2t \cos \frac{2\pi n}{L}, \quad n = 0, 1, \dots, L-1. \quad (10)$$

As a consequence, the energy spectrum ranges from $-2t < E < 2t$ with distinct degrees of degeneracies. The integrated density of states (IDOS) near the bottom of the energy band is shown in Fig. 2 for a set of representative diamond lattices with distinct values of q. The reported results were obtained from lattices with $n = 14$ generations. The vertical segments signal degenerated energies. The regularity of the jumps in the double logarithmic scale shown, which are bounded by an overall power-law growth (dashed lines), reflects the power-law scaling behavior of the degeneracy degree as one approaches the band bottom. Such fractal aspect of the single-particle energy spectrum is commonly obtained in tight-binding quasiperiodic and hierarchical lattices [30–34]. The vanishing of the IDOS at the bottom of the energy band scales as $(E - E_0)^{d_s/2}$, on which the spectral dimension d_s coincides with the fractal dimension d_f of the lattice $[d_s = d_f = \ln(2q)/\ln(2)]$.
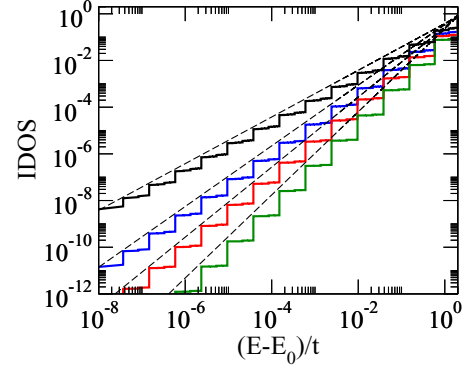

FIG. 2. (Color online) Integrated density of states (IDOS) of the single-particle tight-binding Hamiltonian on hierarchical diamond lattices with distinct number of branches ($q = 2, 3, 4,$ and 6 from bottom to top). Data were obtained from lattices with $n = 14$ generations. Only the behavior near the band bottom is represented. The stepwise form signals the different scales of level degeneracy. The IDOS presents an overall power law, vanishing near the band bottom proportional to $(E - E_0)^{d_s/2}$, with $d_s = d_f = \ln(2q)/\ln(2)$.

III. BOSE-EINSTEIN CONDENSATION IN DIAMOND LATTICES

The possibility of tuning the power-law behavior at the band bottom by changing the branching parameter q of hierarchical diamond lattices opens the possibility to explore distinct thermodynamical regimes of the ideal Bose gas having a finite density of particles distributed on the lattice sites. It is well known that the occurrence of a condensation transition and its critical properties of the ideal Bose gas is strongly dependent of the space dimensionality in homogeneous media [35–37]. In these systems, the spectral dimension d_s coincides with the space dimensionality d. No Bose-Einstein condensation takes place for $d \leqslant 2$, while a mean-field-like transition occurs for $d > 4$ with the specific heat at the transition temperature T_c developing a jump discontinuity and the typical correlation length diverging as $\xi \propto |T - T_c|^{-\nu}$ with $\nu = 1/2$. For intermediate dimensions, one has a non-mean-field transition with specific-heat critical exponent $\alpha = -(4 - d)/(d - 2)$ and $\nu = 1/(d - 2)$. In both mean-field and non-mean-field regimes, the order parameter (measured as the fraction of particles occupying the ground state) vanishes linearly as the transition temperature is approached from below.

Here, we will consider an ideal Bose gas of unitary density having, in average, one particle per lattice site. Without any loss of generality, all eigenenergies will be shifted so that the ground state energy will be set to $E_0 = 0$. The average number of particles occupying a given state $\langle n_i \rangle$ obeys the Bose-Einstein statistics

$$\langle n_i \rangle = \frac{1}{z^{-1} \exp \beta E_i - 1}, \quad (i = 0, 1, \dots N - 1), \quad (11)$$

where $z = \exp(\beta\mu)$ is the fugacity, $\beta = 1/k_B T$, and N is the number of lattice sites. The fugacity can be obtaining by imposing the constraint $N_b = \sum_{i=0}^{N-1} \langle n_i \rangle$, where N_b is the number of bosons present in the network (we consider $N_p = N$ in the following numerical study). The extension of the following results for ideal Bose gases with distinct particle densities is
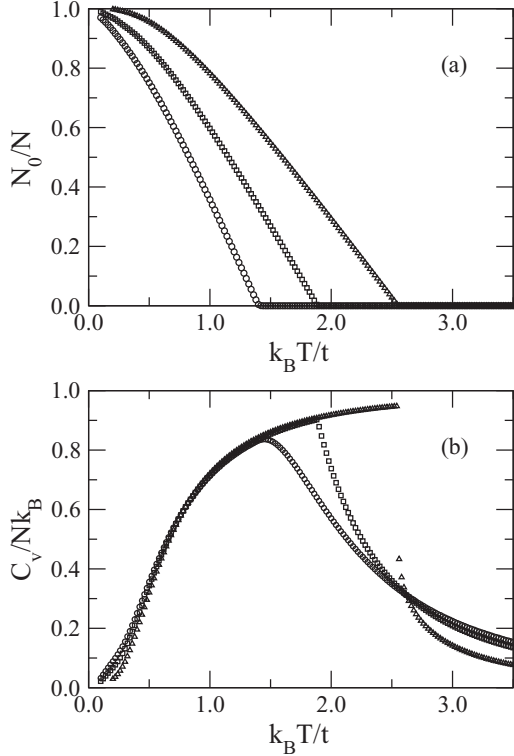
FIG. 3. (a) Condensed fraction N_0/N and (b) Specific heat C_v/Nk_B as a function of temperature for diamond networks with branching parameter $q = 3$ ($d_s = \ln 6/\ln 2 = 2.585$; circles), $q = 4$ ($d_s = \ln 8/\ln 2 = 3$; squares), and $q = 10$ ($d_s = \ln 20/\ln 2 = 4.322$; triangles). Data were obtained from networks with $n = 10$ generations. The condensed fraction vanishes linearly irrespective to the value of the spectral dimension. The specific heat becomes discontinuous for $d_s > 4$ ($q > 8$).

straightforward. Although the transition temperature at which Bose-Einstein condensation occurs monotonically increases with the particle density, the qualitative features associated with the critical behavior of the condensation transition remains the same.

The average number of particles occupying the ground state is given by $N_0 = 1/(z^{-1} - 1)$. We will use the fraction of particles occupying the ground state $\rho = N_0/N$ as the order parameter of the BEC transition. The specific heat C_v can be directly obtained as $C_v = \partial U/\partial T|_N$ where U is the internal energy of the gas given by $U = \sum_{i=0}^{N-1} E_i \langle n_i \rangle$. After a short algebra, it can be put in the form

$$4k_B T^2 C_v = \left[\sum_i E_i^2 \sinh^{-2}(y_i) - \frac{\left[\sum_i E_i \sinh^{-2}(y_i) \right]^2}{\sum_i \sinh^{-2}(y_i)} \right],$$
(12)

with $y_i = (E_i - \mu)/2k_B T$.

In Fig. 3 we plot the condensed fraction and specific heat as a function of temperature for some representative values of the branching parameter $q = 3$, 4, and 10 of the diamond network. These q values correspond, respectively, to spectral dimensions $d_s = 2.585$, 4, and 4.322. Numerical data were obtained from networks with $n = 10$ generations and a unitary
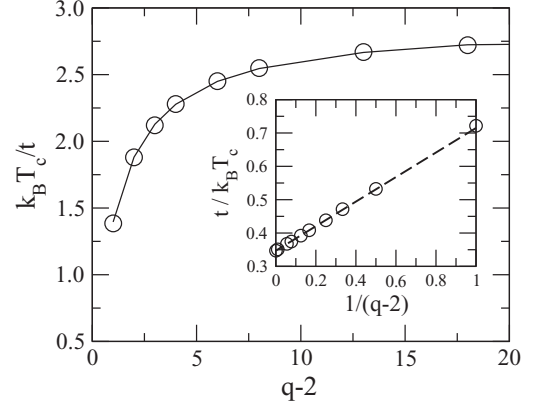

FIG. 4. Transition temperature $k_B T/t$ as a function of the branching parameter q. It saturates at a finite value as $q \to \infty$ while it vanishes as $q \to 2$. Inset: The inverse of the transition temperature as a function of $1/(q - 2)$. The linear fit represents the proposed relation $t/k_B T_c = a + b/(q - 2)$ with $a = (1/\sqrt{6} - 1/6e) = 0.347$ and $b = 1/e = 0.368$.

average number of bosons per site. For $q = 2$ there is no condensed phase. The transition temperature continuously increases with q. The condensed fraction vanishes linearly as the transition is approached, irrespective to the value of q. This result is in agreement with the theoretical prediction that the order parameter critical exponent $\beta = 1$ for the BEC transition. The specific heat depicts distinct trends in the vicinity of the transition. For $q > 8$ ($d_s > 4$) it develops a jump discontinuity at the transition. It becomes continuous at the transition but with a discontinuous first derivative for $4 \leqslant q \leqslant 8$ ($3 \leqslant d_s \leqslant 4$). Finally, for $2 < q < 4$ ($2 < d_s < 3$) its first derivative remains continuous at the transition, with singularities being only present at higher orders. The above regimes are also in agreement with the behavior expected for the specific heat singularity in lattices with power-law spectral density: $\alpha = 0$ (meaning a discontinuity) for $d_s > 4$; $-1 < \alpha < 0$ for $3 < d_s < 4$; and $\alpha < -1$ for $2 < d_s < 3$) [35,36].

The dependence of the transition temperature on the branching parameter q is reported in Fig. 4. It grows monotonically before saturating in the $q \to \infty$ limit. It is interesting to notice that at the onset of the mean-field critical behavior $q = 8$, the transition temperature $k_B T_c/t = \sqrt{6}$ within our numerical accuracy. In the inset, we plot the inverse of the transition temperature versus $1/(q - 2)$. It displays a linear relationship that holds in the entire range of q values. We found that the numerical values of the transition temperature quite closely follow the analytical relation $t/k_B T_c = (1/\sqrt{6} - e^{-1}/6) + e^{-1}/(q - 2)$.

Finally, we performed a finite-size scaling analysis to accurately compute some relevant critical exponents. At the transition temperature, the fraction of condensed particles shall vanish as $N_0/N_b = \rho \propto N^{-\beta/\tilde{\nu}}$. Here $\tilde{\nu} = d_s \nu$. Further, the shift in the specific heat at the transition obeys $\Delta C_v = |C_v(N) - C_v(N \to \infty)| \propto N^{\alpha/\tilde{\nu}}$. The correlation length critical exponent can be estimated from the scaling behavior $\frac{d \ln \rho(T,N)}{dT}|_c \propto N^{1/\tilde{\nu}}$. In Fig. 5, we show the above scaling analysis for the particular case of $q = 3$. All three quantities follow straight power-law behaviors for over six decades, thus
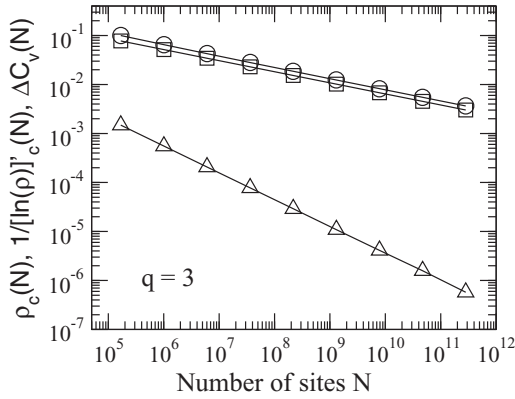
FIG. 5. Scaling behavior at criticality of the order parameter $\rho = N_0/N$ (circles), the inverse of its logarithmic derivative $d \ln \rho/dT$ (squares), and the specific heat shift $\Delta C_v = C_v(N) - C_v(N \to \infty)$ (triangles). Data are from diamond networks with branching parameter $q = 3$. The finite-size scaling exponents are consistent with the expected values for the BEC transition in lattices with spectral dimension $d_s = \ln 6 / \ln 3 = 2.585$, namely $\beta/\tilde{\nu} = 1/\tilde{\nu} = (d_s - 2)/d_s = 0.226$ and $\alpha/\tilde{\nu} = -(d_s - 4)/d_s = -0.547$.

evidencing that corrections to scaling are very small for the system sizes considered. The slopes give the estimates of the critical exponents. The spectral density is $d_s = 2.585 < 4$ for this particular network and, therefore, the critical behavior is non-mean-field like. According to the general theory for the BEC transition of ideal gases, these exponents are expected to be given by $\beta/\tilde{\nu} = 1/\tilde{\nu} = (d_s - 2)/d_s = 0.226$ and $\alpha/\tilde{\nu} = -(4 - d_s)/d_s = -0.547$ [35,36]. The straight lines plotted in Fig. 5 correspond to power laws with these specific exponents and nicely fit the numerical data. We have performed a similar scaling analysis for other values of q and the estimated exponents were always in agreement with the above relations.

IV. SUMMARY AND CONCLUSIONS

In summary, we have characterized the Bose-Einstein condensation transition of noninteracting particles in hierarchical diamond networks. The single-particle Hamiltonian was written within the tight-binding framework, with the hopping amplitude between two neighboring sites of the diamond network being normalized by the geometric average of the respective site connectivities. This procedure was used to keep the bandwidth of the energy eigenvalues finite in the thermodynamic limit.

We demonstrated analytically that, after a proper change of the orthonormal basis set, the single-particle tight-binding Hamiltonian in a hierarchical diamond network with n generations and branching parameter q can be exactly written as a set of decoupled linear chains with a single hopping amplitude t. The sizes and degeneracies of each effective linear chain has been put in terms of the network pair of parameters (q, n), ranging from $(q - 1)(2q)^{n-1}$ single point Hamiltonians up to a single closed chain with 2^{n+1} sites. The proposed transformation allowed us to compute analytically the full spectrum of energy eigenvalues for very large network sizes. In particular, we unveiled that the spectrum has a fractal-like distribution of minibands and gaps. The integrated

density of states (IDOS) has an overall power-law behavior [IDOS $\propto (E - E_0)^{d_s/2}$], with the spectral fractal dimension coinciding with the topological fractal dimension of the underlying diamond network $d_s = d_f = \ln(2q)/\ln(2)$.

The thermodynamics of the ideal gas on diamond networks with distinct branching parameters q was explored, with particular emphasis on the occurrence of a Bose-Einstein condensation (BEC) transition. For networks with $q > 8$ ($d_s > 4$), the BEC transition was shown to be mean-field like, with the specific heat C_v depicting a discontinuity jump at T_c. In the non-mean-field regime, the specific heat is continuous at the transition. Its first derivative remains discontinuous for $4 \leqslant q < 8$ ($3 \leqslant d_s < 4$), while only higher order singularities at C_v are present for $2 < q \leqslant 4$ ($2 < d_s \leqslant 3$). There is no transition for $q = 2$. The transition temperature was shown to monotonically increase with q. We found the numerically estimated values for T_c to closely follow the relation $t/k_B T_c = a + b/(q - 2)$.

A finite-size scaling analysis was employed to estimate the order parameter, correlation length, and specific heat critical exponents. We found that these exponents are, within our numerical accuracy, identical to those on lattices with pure power-law spectral density, namely $\beta/d_s\nu = 1/d_s\nu = (d_s - 2)/d_s$, $\alpha/d_s\nu = -(4 - d_s)/d_s$ for $d_s \leqslant 4$ ($q \leqslant 8$), while they assume mean-field values for $d_s > 4$ ($q > 8$). Therefore, hierarchical diamond networks appear as a simple framework to investigate the critical behavior of the BEC transition in distinct dimensionalities through an exact map onto a set of decoupled linear chains. Future studies of the BEC transition in complex hierarchical networks can bring new insights on how new ingredients such as interparticle interactions and disorder affect the critical behavior in different dimensional regimes.

APPENDIX

We start our proof by illustrating the basic change process in Fig. 6. Suppose that one has a structure as in the left side of Fig. 6. The tight-binding partial Hamiltonian of this subsystem is

$$H_p = t \sum_{h=1}^{q} \sum_{l=1}^{2^m - 2} |h,l\rangle\langle h,l+1| + s|\text{up}\rangle \sum_{h=1}^{q} \langle h, 2^m - 1|$$

$$+ s|\text{down}\rangle \sum_{h=1}^{q} \langle h, 1| + \text{c.c.}, \tag{A1}$$

where c.c. is the complex conjugate. Notice that we use here a different notation with respect to Sec. II: $|\text{up}\rangle$ and $|\text{down}\rangle$ are the two local states corresponding to the up and down nodes in the figure while the other states are numbered according to their horizontal position h and the vertical position l of the corresponding nodes. The up and down nodes are eventually
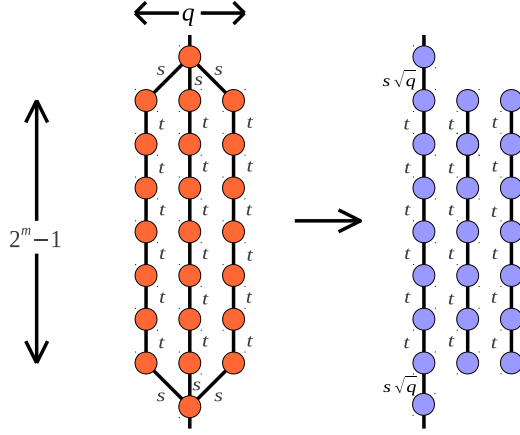
FIG. 6. (Color online) In the figure $q = 3$ and $m = 3$ (therefore, $2^m - 1 = 7$). Notice that m can range from 1 to n. The case $m = 1$ corresponds to the first step of the iteration which allows for the first decomposition of the Hamiltonian which creates $q - 1$ isolated points for any of the $(2q)^{n-1}$ corresponding structures in the diamond.

connected with other parts of the system. We assume orthonormality $\langle r,l|r',l'\rangle = \delta_{r,r'}\delta_{l,l'}$, $\langle \text{up}|\text{up}\rangle = \langle \text{down}|\text{down}\rangle = 1$ and $\langle \text{up}|r,l\rangle = \langle \text{down}|r,l\rangle = \langle \text{up}|\text{down}\rangle = 0$.

It is always possible to transform the orthonormal basis $|r,l\rangle$ in a new orthonormal basis $|\triangleright r,l\rangle$ according to

$$|\triangleright r,l\rangle = \sum_{h=1}^{q} A_{r,h}|h,l\rangle \qquad \text{(A2)}$$

for $1 \leqslant r \leqslant q$, where the $A_{r,h}$ are independent on l, which means that the same transformation is performed at any vertical position in Fig. 6. The $A_{r,h}$ can be always chosen in order that $\langle r,l\triangleleft|\triangleright r',l'\rangle = \delta_{r,r'}\delta_{l,l'}$ (orthonormality) and $A_{L,h} = 1/\sqrt{q}$. With this choice

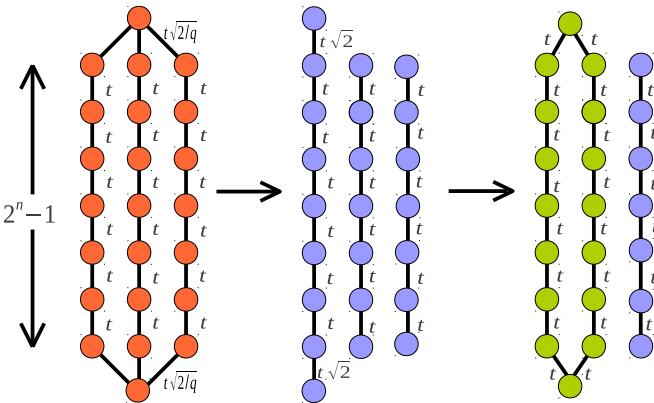$$|\triangleright q,l\rangle = \frac{1}{\sqrt{q}} \sum_{h=1}^{q} |h,l\rangle \qquad \text{(A3)}$$

FIG. 7. (Color online) In the figure $q = 3$ and $n = 3$ (therefore, $2^n - 1 = 7$). The up and down nodes only connect to the shown nodes. The transformation is made once involving all q columns and then backward involving only the first two columns.

and the partial Hamiltonian (13) rewrites as

$$H_p = t \sum_{h=1}^{q} \sum_{l=1}^{2^m-2} (|\triangleright h,l\rangle\langle h,l+1\triangleleft| + s\sqrt{q} \; |\text{up}\rangle \langle q,2^m-1\triangleleft|$$

$$+ s\sqrt{q} \, |\text{down}\rangle \langle q,1\triangleleft|) + \text{c.c.}, \qquad \text{(A4)}$$

which corresponds exactly to the system in the right-hand side of Fig. 6 since the up and down nodes are only connected to a single spin in the subsystem (while eventually remaining connected to other parts of the system).

Now we observe that the diamond network of generation n has initially $(2q)^{n-1}$ structures as in the left-hand side of Fig. 6 corresponding to $m = 1$. Therefore, the first step of the iteration creates $g(1) = (q-1)(2q)^{n-1}$ isolated points.

Since the connectivity of each node is updated by a factor q at any new generation and the connectivity of each new created node equals 2, we immediately observe that, after the first iteration, the new network has $(2q)^{n-2}$ structures as in the right-hand side of Fig. 6 correspondingly to $m = 2$. Therefore, the second step of the iteration creates $g(2) = (q-1)(2q)^{n-2}$ open chains of length $2^2 - 1 = 3$.

The procedure can be iterated until one remains with $g(m)$ open chains of length m for any $1 \leqslant m \leqslant n-1$ plus the structure which is shown in the left-hand side of Fig. 7. This structure is analogous to the structure shown in Fig. 6 with the difference that now up and down nodes correspond to the two initial nodes and they have only connections shown in the figure. Also notice that now the vertical length is $2^n - 1$ where
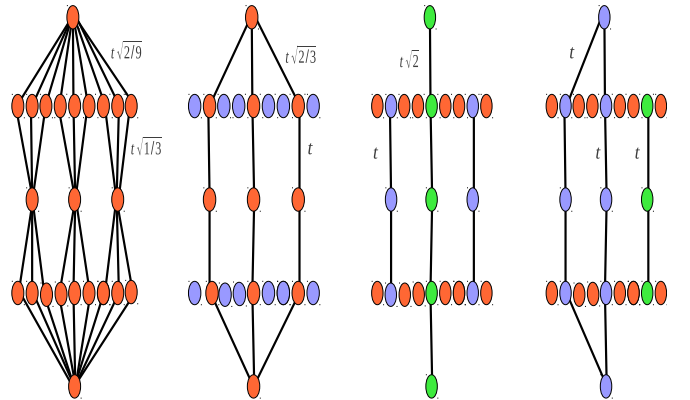

FIG. 8. (Color online) In the figure $q = 3$ and $n = 2$. The hopping energies of the diamond have two possible values: $t\sqrt{2/9}$ (bonds connecting the two initial nodes) and $t\sqrt{1/3}$ (other bonds). After the first step $g(1) = (q-1)(2q)^{n-1} = 12$ isolated nodes are created and a structure with hopping energies with two possible values: $t\sqrt{2/3}$ (bonds connecting the two initial nodes) and t (other bonds). After the third step, the structure is replaced by two open chains of length $2^n - 1$ with all having hopping energies t and one open chain of length $2^n + 1$ with hopping energies with two possible values: $t\sqrt{2}$ (bonds connecting the two initial nodes) and t (other bonds). After the final step, one open chain of length $2^n - 1$ and the open chain of length $2^n + 1$ are replaced by a single periodic chain of length 2^{n+1} and hopping energies t. The final result is a collection of various chains of different sizes, all of them having a single hopping energy t.

n is the generation number of the network. Their hopping energy is $t\sqrt{2/q}$ with each of their q connected nodes.

At this point, one can proceed as in (A1)–(A4) and show that the system is equivalent to the system shown in the central part of Fig. 7.

The final step of our proof is now very simple since one can consider the first two open chains of lengths $2^n + 1$ and $2^n - 1$ respectively and perform backward the transformation (A1)–(A4) only on these two chains. The final result, shown

at the right hand side of Fig. 7, consists in $q - 2$ open chains of length $2^n - 1$ and a single periodic chain of length 2^{n+1}.

Finally the result is that the (q legs, generation n) diamond Hamiltonian is equivalent to the Hamiltonian of a system composed by $g(m) = (q - 1)(2q)^{n-m}$ open chains of length m for any $1 \leqslant m \leqslant n - 1$, $q - 2$ open chains of length $2^n - 1$ and a single periodic chain of length 2^{n+1}. The complete procedure is illustrated in Fig. 8 in the case $q = 3$ and $n = 2$.

[1] A. N. Berker and S. Ostlund, J. Phys. C **12**, 4961 (1979).

[2] R. B. Griffiths and M. Kaufman, Phys. Rev. B **26**, 5022 (1982).

[3] M. Kaufman and R. B. Griffiths, Phys. Rev. B **24**, 496 (1981).

[4] M. Kaufman, Phys. Rev. B **30**, 413 (1984).

[5] M. Kaufman, T. Berger, P. D. Gujrati, and D. Bowman, Phys. Rev. A **41**, 4371 (1990).

[6] M. Kaufman and D. Andelman, Phys. Rev. B **29**, 4010 (1984).

[7] Z. R. Yang, Phys. Rev. B **38**, 728 (1988).

[8] Y. Qin and Z. R. Yang, Phys. Rev. B **43**, 8576 (1991).

[9] Z.-Z. Zhang, S.-G. Zhou, and T. Zou, Eur. Phys. J. B **56**, 259 (2007).

[10] F. Iglói and L. Turban, Phys. Rev. B **80**, 134201 (2009).

[11] A. Eddi, A. Decelle, E. Fort, and Y. Couder, Europhys. Lett. **87**, 56002 (2009).

[12] L. Zdeborová, A. Decelle, and M. Chertkov, Phys. Rev. E **80**, 046112 (2009).

[13] M. Castellana, A. Decelle, S. Franz, M. Mézard, and G. Parisi, Phys. Rev. Lett. **104**, 127206 (2010).

[14] D. O. C. Santos, E. Nogueira, Jr., and R. F. S. Andrade, Phys. Rev. B **73**, 174202 (2006).

[15] A. Decelle, F. Krzakala, C. Moore, and L. Zdeborová, Phys. Rev. Lett. **107**, 065701 (2011).

[16] I. N. de Oliveira, F. A. B. F. de Moura, M. L. Lyra, J. S. Andrade, Jr., and E. L. Albuquerque, Phys. Rev. E **79**, 016104 (2009).

[17] I. N. de Oliveira, F. A. B. F. de Moura, M. L. Lyra, and J. S. Andrade, Jr., and E. L. Albuquerque, Phys. Rev. E **81**, 030104(R) (2010).

[18] R. Burioni, D. Cassi, I. Meccoli, M. Rasetti, S. Regina, P. Sodano, and A. Vezzani, Europhys. Lett. **52**, 251 (2000).

[19] R. Burioni, D. Cassi, M. Rasetti, P. Sodano, and A. Vezzani, J. Phys. B: At. Mol. Opt. Phys. **34**, 4697 (2001).

[20] P. Buonsante, R. Burioni, D. Cassi, and A. Vezzani, Phys. Rev. B **66**, 094207 (2002).

[21] R. Burioni, D. Cassi, and A. Vezzani, J. Phys. A: Math. Gen. **35**, 1245 (2002).

[22] I. Brunelli, G. Giusiano, F. P. Mancini, P. Sodano, and A. Trombettoni, J. Phys. B: At. Mol. Opt. Phys. **37**, S275 (2004).

[23] P. Sodano, A. Trombettoni, P. Silvestrini, R. Russo, and B. Ruggiero, New J. Phys. **8**, 327 (2006).

[24] M. Lorenzo, M. Lucci, V. Merlo, I. Ottaviani, M. Salvato, M. Cirillo, F. Müller, T. Weimann, M. G. Castellano, F. Chiarello, and G. Torrioli, Phys. Lett. A**378**, 655 (2014).

[25] I. N. de Oliveira, T. B. dos Santos, F. A. B. F. de Moura, M. L. Lyra, and M. Serva, Phys. Rev. E **88**, 022139 (2013).

[26] M. Serva, arXiv:1402.4661.

[27] S. Sil, S. K. Maiti, and A. Chakrabarti, Phys. Rev. Lett. **101**, 076803 (2008).

[28] S. Sil, S. K. Maiti, and A. Chakrabarti, Phys. Rev. B **78**, 113103 (2008).

[29] A. Rodriguez, A. Chakrabarti, and R. A. Romer, Phys. Rev. B **86**, 085119 (2012).

[30] X. Fu, Y. Liu, Z. Guo, P. Zhou, and X. Huang, Phys. Rev. B **51**, 3910 (1995).

[31] E. Macia and F. Dominguez-Adame, Semicond. Sci. Technol. **11**, 1041 (1996).

[32] E. S. Zijlstra, A. Fasolino, and T. Janssen, Phys. Rev. B **59**, 302 (1999).

[33] W. A. Schwalm and B. J. Moritz, Phys. Rev. B **71**, 134207 (2005).

[34] E. Macia, Phys. Rev. B **74**, 245105 (2006).

[35] J. D. Gunton and M. J. Buckingham, Phys. Rev. **166**, 152 (1968).

[36] C. K. Hall, J. Stat. Phys. **13**, 157 (1975).

[37] R. Beckmann, F. Karsch, and D. E. Miller, Phys. Rev. A **25**, 561 (1982).